Statistical response of middle atmosphere composition to solar proton events in WACCM-D simulations: importance of lower ionospheric chemistry

Niilo Kalakoski[1], Pekka T. Verronen[1,2], Annika Seppälä[3], Monika E. Szeląg[1,*], Antti Kero[2], and Daniel R. Marsh[4,5]

[1]Space and Earth Observation Centre, Finnish Meteorological Institute, Helsinki, Finland
[2]Sodankylä Geophysical Observatory, University of Oulu, Sodankylä, Finland
[3]Department of Physics, University of Otago, Dunedin, New Zealand
[4]Atmospheric Chemistry Observations and Modeling, National Center for Atmospheric Research, Boulder, CO, USA
[5]Priestley International Centre for Climate, University of Leeds, Leeds, UK
[*]earlier known as M. E. Andersson

Correspondence: Niilo Kalakoski (niilo.kalakoski@fmi.fi)

Abstract. Atmospheric effects of solar proton events (SPE) have been studied for decades, because their drastic impact can be used to test our understanding of upper stratospheric and mesospheric chemistry in the polar cap regions. For example, odd hydrogen and odd nitrogen are produced during SPEs, which leads to depletion of ozone in catalytic reactions, such that the effects are easily observed from satellites during the strongest events. Until recently, the complexity of the ion chemistry in the lower ionosphere (i.e. in the D region) has restricted global models to simplified parameterizations of chemical impacts induced by energetic particle precipitation (EPP). Because of this restriction, global models have been unable to correctly reproduce some important effects, such as the increase of mesospheric HNO_3 or the changes in chlorine species. Here we use simulations from the WACCM-D model, a variant of the Whole Atmosphere Community Climate Model, to study the statistical response of the atmosphere to the 66 strongest SPEs which occurred in the years 1989–2012. Our model includes a set of D-region ion chemistry, designed for a detailed representation of the atmospheric effects of SPEs and EPP in general. We use superposed epoch analysis to study changes in O_3, HO_x ($OH + HO_2$), Cl_x ($Cl + ClO$), HNO_3, NO_x ($NO + NO_2$) and H_2O. Compared to the standard WACCM which uses an ion chemistry parameterization, WACCM-D produces a larger response in O_3 and NO_x, a weaker response in HO_x and introduces changes in HNO_3 and Cl_x. These differences between WACCM and WACCM-D highlight the importance of including ion chemistry reactions in models used to study EPP.

1 Introduction

Solar proton events (SPEs) are observed on Earth when high-energy protons accelerated in the sun's magnetic field during a solar coronal mass ejection strike Earth. These protons generally have energies in the range of tens or hundreds of MeVs/nucleon and due to their high energies are able to penetrate deep into the atmosphere at geomagnetic latitudes polewards of $\approx 60°$. This causes ionization and dissociation (mainly of the most abundant species N_2 and O_2) in the altitude range of roughly 30–90 km.

Solar proton events typically last from a few hours to few days and can occur anytime during the 11-year solar cycle, although they are more common during solar maximum.

Ionization, excitation and dissociation caused by the SPEs, and energetic particle precipitation (EPP) in general, have a significant influence on neutral composition through ion-neutral chemistry (e.g. Verronen and Lehmann, 2013). Several studies have investigated the depletion of ozone in the polar mesosphere and upper stratosphere resulting from the increased production of odd hydrogen and odd nitrogen (e.g. Jackman et al., 2001; Seppälä et al., 2004; López-Puertas et al., 2005; Verronen et al., 2006). Ozone depletion can result in changes in temperatures during the largest SPEs (Jackman et al., 2007), and there is evidence that SPEs, as part of EPP, can modulate polar winter dynamics on decadal time scales (Seppälä et al., 2009; Semeniuk et al., 2011; Rozanov et al., 2012; Calisto et al., 2013). Recent results have also shown that SPEs play a role in upper stratospheric variability of ozone and have to be considered when studying the expected recovery of the ozone layer (Stone et al., 2018). State of art on the impact of energetic particle precipitation, in particular SPE and geomagnetic forcing, has also been summarized in the recent WMO assessment (WMO, 2018, chapter 4.3.5.1, page 4-25, and references therein).

Simulation results have suggested that the decrease of polar total ozone column would be of the order of 1–2% a few months after large SPEs (Jackman et al., 2014). However, local depletion has been reported to reach $\approx$10% below the ozone layer peak at 50–100 hPa, based on a statistical analysis of almost 200 SPEs using ozone soundings (Denton et al., 2018). As the contribution of >300 MeV protons to direct ozone loss in the lower stratosphere would likely be negligible due to the relatively small fluxes at such high energies (Jackman et al., 2011), any observed ozone loss would likely be the result of indirect effects. Ozone may also increase in the lower stratosphere due to the enhanced NO_x interfering with chlorine-driven catalytic ozone loss (Jackman et al., 2008).

The lower ionospheric, the D-region, chemistry, which connects SPE ionization to changes in neutral species, is rather complex compared to the 5-ion chemistry that is adequate in the thermosphere. A special feature of the D-region is the presence of negative ions which are formed when electrons attach to neutral species. Another feature is the large number of different cluster ions, both positive and negative, some of which are among the most abundant ions in the region. Due to the large number of D-region ions and ionic reactions, atmospheric models have typically included the SPE, or EPP, effects using simple parameterizations of HO_x and NO_x production.

Funke et al. (2011) discussed shortcomings related to these parameterization schemes in a comparison study between observations and simulations of the October-November 2003 SPE. Among the outstanding issues in simulations have been the lack of nitric acid, HNO_3, increase (see also Jackman et al., 2008), as well as lack of chlorine activation. The HNO_3 production is driven through reactive nitrogen redistribution by negative ion chemistry (Verronen and Lehmann, 2013), and simulations could be improved either by improved parameterization (Päivärinta et al., 2016), or by considering the relevant ion chemistry explicitly (Verronen et al., 2008; Verronen et al., 2011; Andersson et al., 2016). The differences between modeled and observed response of chlorine species to SPE reported by Jackman et al. (2008) can be explained by the conversion of HCl to active chlorine species (Cl, ClO, HOCl) by the ion chemical reactions (Winkler et al., 2009, 2011). In the lower ionosphere, the ion chemistry reactions are expected to lead to the depletion of water vapour during SPEs. For moderate sized SPEs, this effect

is small compared to the icy particle sublimation governed by the changes in temperature (von Savigny et al., 2007; Winkler et al., 2012).

The Whole Atmosphere Community Climate Model (WACCM) is a global chemistry-climate model and forms the atmospheric part of the Community Earth System Model (CESM). Recently, a variant called WACCM-D was developed for detailed simulations of D-region ion chemistry and EPP atmospheric effects (Verronen et al., 2016). In a case study of the January 2005 SPE, the consideration of ion chemistry in WACCM-D led to an improved SPE response in HNO_3, Cl_x, NO_x, and HO_x (Andersson et al., 2016). Since then, WACCM-D has been used to study mesospheric nitric acid and cluster ion composition during electron precipitation events (Orsolini et al., 2018) and magnetic latitude dependency of SPE ionospheric impact (Heino et al., 2019).

Here, we take a statistical approach to look at the response of middle atmosphere chemistry to a number of SPEs of various intensities. As the SPE effects are largely known from previous work, we focus on the improvement provided by additional ion chemistry reactions included in the WACCM-D chemistry. In addition to the traditionally analyzed species, such as O_3, HO_x, NO_x and HNO_3, we also investigate water vapour and active chlorine species which have been less studied, especially with global models. While several of the largest SPEs included in the analysis have previously been studied individually, the statistical approach used here allows for inclusion of a number of moderate sized events in various background atmosphere and illumination conditions. This approach also allows for identification of climatological effects above natural variability. As the analysis includes SPEs of different sizes occuring during different seasons, a statistical approach is most useful for study of temporal and spatial extent, rather than magnitude of the response.

2 Modeling and analysis methods

2.1 WACCM-D simulations

WACCM is a global circulation model with fully coupled chemistry and dynamics extending from surface to 6×10^{-6} hPa ($\approx$140 km). The horizontal resolution used is 1.9° latitude by 2.5° longitude. A description of the model physics in the MLT (mesosphere-lower thermosphere) as well as the simulations of dynamical and chemical response to radiative and geomagnetic forcing during solar maximum and minimum are described by Marsh et al. (2007). Marsh et al. (2013) presents an overview of the model climate and describes the climate and the variability in a long-term simulation using version 4 of the WACCM. The standard chemistry package of WACCM includes photochemistry of 59 neutral species for the whole altitude range, and five ion species O^+, NO^+, O_2^+, N_2^+ and N^+ for the lower thermosphere, as well as excited species $N(^2D)$, $O(^1D)$, $O_2(^1\Delta)$ and $O_2(^1\Sigma)$. For SPE effects, and energetic particle precipitation in general, HO_x and NO_x production is parameterized. For the SPE NO_x effect, it is assumed that 1.25 N atoms are produced per ion pair with branching ratios of 0.55/0.7 for $N(^4S)/N(^2D)$, respectively (Jackman et al., 2005; Porter et al., 1976). This parameterization depends on a fundamental assumption of fixed N_2 / O_2 ratio, and it has been shown to underestimate NO_x production above about 65 km (Nieder et al., 2014; Andersson et al., 2016). For the SPE HO_x effect, based on the work of Solomon et al. (1981), a maximum of two molecules are produced

per ion pair in the lower mesosphere and below while in the upper mesosphere the production gradually decreases to zero with increasing altitude.

WACCM-D is a variant of WACCM in which the standard parameterizations of HO_x and NO_x production are replaced by a set of lower ionospheric photochemistry, with the aim to reproduce better the observed effects of EPP on the mesosphere and upper stratosphere neutral composition. The ion chemistry set was selected based on analysis of the latest knowledge of chemical reactions in the ionospheric D-region and their effects on the neutral atmosphere (Verronen and Lehmann, 2013). The set consists of 307 reactions of 20 positive ions and 21 negative ions, including cluster ions such as $H^+(H_2O)$ and $NO_3^-(HNO_3)$ which are important for, e.g., HO_x and HNO_3 production. The details on WACCM-D ion chemistry as well as its lower ionospheric evaluation were presented by Verronen et al. (2016), while the improvement in the atmospheric response during the January 2005 SPE was demonstrated in comparisons with satellite observations (Andersson et al., 2016). WACCM-D is now included as an official predefined component set (compset) since the CESM 2.0 release in June 2018.

In this study, we use WACCM version 4 simulations with the specified dynamics configuration (SD-WACCM) which is forced with meteorological fields (temperature, horizontal winds, and surface pressure) from NASA's Modern-Era Retrospective Analysis for Research and Applications (MERRA) (Rienecker et al., 2011; Lamarque et al., 2012) at every dynamics time step below about 50 km; above this, the model is free running (88 levels in total). It should be noted that even above 50 km model dynamics are strongly modulated by winds and wave fluxes from lower levels. This means that internal variability of dynamics in SD-WACCM is small.

For energetic particle precipitation, the simulations include forcing from auroral electrons ($E < 10$ keV), solar protons, and galactic cosmic rays. Medium-energy and high-energy electrons ($E > 10$ keV) were excluded from the simulations. Two model simulations were made: (1) a reference run using standard SD-WACCM compset (referred to as REF) and (2) a run with D-region ion chemistry (referred to as WD). Both simulations covered the years 1989 to 2012. We use daily mean SPE ionization rates based on GOES (Geostationary Operational Environmental Satellite) observations and described, e.g., in Jackman et al. (2011). The energy range for protons is 1–300 MeV, thus the direct atmospheric impact takes place at altitudes above ≈ 10 hPa (e,g, Turunen et al., 2009, Figure 3).

Proton fluxes were only included for energies up to 300 MeV. However, Jackman et al. (2011) show that higher energies contribute very little to the total ozone or NO_y impact. We only consider protons, and not the X-ray flares that are associated with some SPEs - in the polar regions we can assume that the proton effect is the dominant one, at least for large SPEs (Pettit et al., 2018).

2.2 Analysis methods

For our statistical analysis, SPEs were selected using proton flux data from satellite-based GOES observations (available from https://www.ngdc.noaa.gov/stp/satellite/goes/index.html). An event was selected if the peak proton flux exceeded 100 particle flux units (pfu), with pfu defined as the five-minute average flux in units of particles $cm^{-2}s^{-1}sr^{-1}$ for protons with energy larger than 10 MeV. To avoid obscuring the signal in composite means by introducing duplicates of major events in days preceding the zero epoch date, any event following a larger event onset within seven days was excluded from the analysis. In

total, eleven such events were removed. Following these criteria, 66 events given in Table A1 were identified in the simulation period. The seasonal distribution of the selected SPEs is shown in Figure 1. As SPEs are sporadic, the distribution is somewhat uneven, with the northern hemisphere winter months (Dec – Feb) underrepresented. Of the 8 largest SPEs (above 10000 pfu) in the analysis, five occurred October or November, compared to only each in March, July and September.

Table 1. Definitions used in the text for the SD-WACCM and WACCM-D simulations.

REF	Daily mixing ratios from the standard SD-WACCM simulation.
$\overline{REF}$	Daily climatological (1989-2012) mean mixing ratios from the standard SD-WACCM simulation.
$\widehat{REF} = REF - \overline{REF}$	Daily mixing ratio anomalies from the standard SD-WACCM simulation.
WD	Daily mixing ratios from the WACCM-D simulation.
$\overline{WD}$	Daily climatological (1989-2012) mean mixing ratios from the WACCM-D simulation.
$\widehat{WD} = WD - \overline{WD}$	Daily mixing ratio anomalies from the WACCM-D simulation.
Composite mean	Mean over the 66 individual cases.

5   For each of the 66 events, zero epoch day (D_0) was defined as the first day when the proton flux exceeded 10 pfu. A 90-day epoch period around the zero epoch ($[D_0 - 29, D_0 + 60]$) was selected from the daily mean time-series for the following constituents: O_3, HO_x ($OH + HO_2$), Cl_x ($Cl + ClO$), HNO_3, NO_x ($NO + NO_2$) and H_2O. Definitions of abbreviations used in the following text for the statistical quantities from REF and WD simulations are shown in table 1.

    To assess the anomalies $\widehat{REF}$ and $\widehat{WD}$ associated with the SPEs, daily climatological mean mixing ratios $\overline{REF}$ and $\overline{WD}$ were

10   deducted from respective epoch mixing ratios REF and WD. Figure 2 shows the composite means of $\overline{WD}$ for northern polar cap (60–90 °N, area-weighted). Note that due to the seasonal distribution of the events some seasonal signals remain visible in the composite means, e.g. slight increase of mesospheric O_3 during the 90-day epoch period. It can also been seen that for some constituents, especially HNO_3, mixing ratio enhancements following the events are large enough to visibly affect the daily climatology.

15   For each constituent, we calculate the composite mean of difference μ_d between the epoch time series and the corresponding climatological time series

$$\mu_d = \frac{\sum_{i=1}^{66}(r(t_i) - c(t_i))}{66}, \quad t_i = D_{0_i} + d,$$

where r is the relevant mixing ratio epoch time series REF or WD, c is the epoch time series from daily climatology $\overline{REF}$ or $\overline{WD}$, and d the number of days before and after zero epoch D_{0_i}. Subtracting the climatological values from the epoch time

20   series helps to separate the SPE signal from the seasonal signals which can arise from the uneven monthly distribution of the SPEs (see Figure 1). Variance of the composite means was approximated by bootstrapping, i.e. by re-sampling the random selection of dates 1000 times with replacement, with N = 66 for each sample. Bootstrapping was chosen for variance estimation due to its independence of the shape of the distribution, i.e. it does not require a normal distribution. The standard deviation

of the variance was then used to identify robust responses, i.e. SPE-driven changes that are clearly larger than the normal variability.

The SPE-driven anomalies are expected to occur following the SPE onset (zero epoch). However, in Section 3 we will show that the results sometimes have also anomalies that extend over the full epoch period. These anomalies are in most cases related to solar cycle variability, due to the SPE sampling over-representing the solar cycle maximum years when compared to climatology. Composite mean SPE ionization for the analyzed epochs is shown in Figure 3. Daily composite mean peak ionisation is 891 ion pairs/cm^3/s, which is roughly similar in magnitude to peak ionisation associated with January 2005 SPE. Largest individual events in the time series feature peak ionisations about ten times higher, for example peak ionisation of 8534 ion pairs/cm^3/s for the Halloween SPE. In addition to main ionization peak within ca. 5 days following the onset of the SPE, secondary ionization peaks are evident in the epoch mean, due to closely separated SPEs. While these secondary peaks are much weaker (by roughly an order of magnitude) than the main peak, they can still cause noticeable anomalies in some of the analyzed constituents.

In order to evaluate the contribution of the improved ion chemistry of WACCM-D, the same epoch analysis was made for both the REF and the WD simulations. The anomalies from the WACCM-D simulation ($\widehat{WD}$) were then compared to anomalies from the standard WACCM ($\widehat{REF}$) (Figures 4 and 5). We considered the difference of composite means of differences in mixing ratio between the two simulations for full altitude range (Figures 6 and 7) as well as comparison of the SPE response at pressure levels chosen for maximum difference between two simulations (Figures 8 and 9).

3 Results and discussion

3.1 Statistical response from WACCM-D

Figures 4 (Northern Hemisphere, NH) and 5 (Southern Hemisphere, SH) show the mean anomaly of the super-imposed epochs for O_3, HO_x, Cl_x, HNO_3, NO_x and H_2O. Statistically robust anomalies, i.e. those larger than two times the standard deviation of the bootstrap variance, are shown in color and discussed below.

Several constituents show the most pronounced anomaly immediately following the event onset (zero epoch) which in the figures is marked with a black vertical line. For some constituents, most notably H_2O and Cl_x, persistent anomalies extending throughout the epoch period are seen as well. These anomalies can be considered to represent the solar cycle signal because the distribution of SPEs concentrates on the years around the solar maximum. Some anomalies are clearly affected by the response to closely separated SPEs, i.e. when the separation is smaller than 60 days. These are most notable in NO_x and HMO_3 in NH around days -15, $+22$ and $+45$ wrt. to zero epoch, corresponding to the secondary peaks of SPE ionization (see Figure 3).

Ozone (top-left panel, Figures 4 and 5) decreases between 1 and 0.01 hPa immediately following the SPE, lasting about 5–10 days. This is caused by catalytic destruction from enhanced HO_x. Ozone loss also takes place around 1 hPa, driven by NO_x and Cl_x. The depletion around 1 hPa lasts much longer, driven by the NO_x increase, with maximum ozone decrease seen about 30 days after the event onset. In contrast, an increase of ozone is seen throughout the period near the secondary ozone maximum above 0.01 hPa, more robustly in the southern hemisphere. This increase is linked to enhanced atomic oxygen production by

O$_2$ photolysis in solar maximum conditions (see also Marsh et al., 2007). In the stratosphere below 5 hPa the ozone response is not consistently robust. However, an intermittent increase, likely caused by solar cycle effects, is seen throughout the epoch period in this region. Thus the decrease of total ozone column, as reported by Denton et al. (2018), is not seen in our analysis. It should be noted that the highest energy protons ($E >$300 MeV), which can directly impact the lower stratosphere, are not included in the particle forcing used in our simulations. However, it is not clear if inclusion of these protons would change the response because their fluxes should be too low to cause a significant extra response (Jackman et al., 2011).

Strong, short-lived increase of HO$_x$ is seen below 0.01 hPa (top-center panels) immediately following the SPE, reaching down to the 10 hPa level, with the strongest and the most robust response in the mesosphere. Due to the short chemical lifetime of HO$_x$, there is no longer-term anomaly beyond 10 days from the SPE onset. The later peaks just below 0.01 hPa are caused by SPEs occurring within 60 days of zero epoch of analysed SPE. Above 0.01 hPa, a small negative anomaly is present throughout the period, related to solar maximum through less water vapour in the region and lowering of the HO$_x$ peak altitude. The persistent positive anomaly at just below 0.01 hPa, seen in the SH, is consistent with lowering of the HO$_x$ peak altitude. Factors affecting HO$_x$ peak altitude during solar maxima are the decrease of H$_2$O and the increase of Lyman-α photolysis, balancing at the level of mesopause.

Cl$_x$ mixing ratios (top-right panels) are enhanced between 1 and 0.01 hPa, these SPE-driven increases last up to about a week. Below 1 hPa, at the altitude of Cl$_x$ mixing ratio maximum, Cl$_x$ is a reduced. This decrease is roughly consistent and continuos throughout the epoch period, so is likely, at least in part, connected to the solar cycle rather than individual events. However, the magnitude of the negative anomaly increases following the onset of the SPE, with maximum value in the SH reached after 30 days. Short-lived decrease of the NH polar upper stratosphere ClO during the January 2005 SPE has previously been reported both in satellite observations and models (Damiani et al., 2012; Andersson et al., 2016). In short term decrease is likely caused by conversion of ClO to HOCl in the presence of enhanced HO$_2$, while in the longer term, the decrease is probably connected to descent of NO$_x$ and subsequent formation of ClONO$_2$. Here we look at the polar average, but it should be noted that in the presence of SPE-generated HO$_x$, response of Cl$_x$ in the polar atmosphere depends strongly on the sunlight conditions and varies across latitudes and altitudes (Funke et al., 2011). For example, in polar night stratosphere ClO is converted to HOCl in reaction with HO$_2$, while in daytime HOCl is converted to ClO by OH.

Large increase in HNO$_3$ (bottom-left panels) is seen up to 10 days after the SPE onset, with a maximum between 1–0.01 hPa. The absence of a longer-term effect is due to the fast photodissociation of HNO$_3$ in sunlit conditions. Similar to HO$_x$, the later peaks around days 20 and 45 in the NH are caused by nearly coincident SPEs. A longer-term enhancement persists for 20–30 days after SPEs below 1 hPa. The anomalies are weaker in the SH than in the NH, due to the strongest SPEs mostly occurring during NH winter (see Figure 1) when there is less solar radiation and HNO$_3$ photodissociation.

SPE-driven enhancements of NO$_x$ (bottom-center panels) reach down to 1 hPa level and below. These enhancements start to diminish after about 10 days, but robust longer-term enhancements can be seen for several weeks afterwards. This is especially clear at lower altitudes (around 1 hPa), where transport from above contributes to persistence of enhancements. The response is different in the northern and southern hemispheres due to the seasonal distribution of the events. In the NH, several strong, closely separated winter-time events show up as recurring anomalies, which are then transported to lower altitudes. The SH

response is less variable, with small but robust enhancements seen through the two months following the SPE onset. In addition to the SPE-driven anomaly, there is a persistent, underlying anomaly seen above about 10 hPa from enhanced NO_x production in the lower thermosphere by solar EUV and EPP during solar maximum times (see also Marsh et al., 2007).

During an SPE, H_2O would be expected to decrease when it is converted to HO_x in ionic reactions. In our analysis, H_2O (bottom-right panels) shows consistent and statistically robust negative anomaly throughout the period analysed, except in the SH lower stratosphere. There is some indication of a stronger anomaly following the SPEs above 0.1 hPa, i.e. at altitudes where HO_x increases. But in general the anomaly is mostly related to the solar cycle through the increased Lyman-α photodissociation during solar maximum decreasing H_2O in the mesosphere-lower thermosphere (see also Schmidt et al., 2006; Marsh et al., 2007).

3.2 Effects of D-region ion chemistry

Figures 6 and 7 show the difference between epoch responses in the NH and SH, respectively, from WACCM-D and the standard WACCM. As the specified dynamics of the two simulations are identical, differences seen in these figures arise from the addition of the D-region ion chemistry. Note that the robustness threshold for these figures is set to one standard deviation rather than the two standard deviations used in Figures 4 and 5. The differences shown in figures for constituents other than O_3 and H_2O also satisfy the two standard deviation threshold. The effects on O_3 and H_2O, however, do not reach the two standard deviation threshold. Further, Figures 8 and 9 show line plots of epoch response from both WACCM-D ($\widehat{WD}$) and standard WACCM ($\widehat{REF}$) at pressure levels corresponding to maximum significant difference in Figures 6 and 7.

Ozone (top-left panels) depletion is larger in WACCM-D for about 5 days after the onset at around 0.5–1 hPa. This effect is very similar in both hemispheres. Both the duration and altitude range of this extra ozone loss clearly correspond to enhanced Cl_x, while there is no clear connection to NO_x or HO_x differences. Less ozone depletion takes place in WACCM-D around 0.01 hPa level, connected to the clearly lower HOx enhancement in WACCM-D. Anomaly of similar magnitude is observed in both hemispheres, although it is only robust in SH. The reduced HO_x response in WACCM-D is a result of the lower water vapor amount, and thus lower HO_x production, than what is assumed when HO_x production is parameterized (Andersson et al., 2016).

Cl_x is enhanced in both hemispheres above 1 hPa in WACCM-D, while there is only a relatively weak increase in the standard WACCM. The reasons for the enhancement are the ion reactions included in WACCM-D that convert more HCl to active chlorine species Cl and ClO (Winkler et al., 2009) than the neutral gas-phase reactions which are included in both standard WACCM and WACCM-D. Enhancements relating to secondary ionization peaks can also be seen, most clearly around day 40. The negative anomaly of Cl_x below 1 hPa seen in Figures 4 and 5 is not present here, again implying that this anomaly is not predominantly due to ion chemistry.

The HNO_3 enhancement is clear and strong in WACCM-D, as ion chemistry produces it from other NO_y species. Standard WACCM, like other models using an EPP lookup table parameterization, is known to underestimate the HNO_3 mixing ratios when compared to observations (Jackman et al., 2008; Funke et al., 2011; Andersson et al., 2016). A discrepancy between

WACCM-D and standard WACCM HNO_3 enhancements is clearly seen in Figures 8 and 9. Due to the dramatic increase on HNO_3 following SPEs, peaks from other, close-by events are also clearly seen in Figure 8.

In the mesosphere, the NO_x enhancement is much larger in WACCM-D than in standard WACCM. Below 0.1 hPa there are some signs of an increase in transported NO_x, although this effect is not statistically robust. Increased NO_x is consistent between the hemispheres. Andersson et al. (2016) attributes the increased NO_x to enhanced production above 80 km (ca. 0.01 hPa), mostly due to the reaction $O_2^+ + N_2 \rightarrow NO^+ + NO$, and consequent transport to lower altitudes.

Differences in H_2O anomalies (Figures 6–9, lower-right panels) between WACCM-D and the standard WACCM are seen above 1.0 hPa but they are almost entirely overcome by the variance, which indicates that negative anomalies in Figures 4 and 5 are not primarily connected to ion chemistry reactions but are a solar cycle signal. However, a short-lived negative difference , robust to $1\sigma-$ level, can be seen at 0.01 hPa immediately following the onset of SPE, even though the co-located HO_x production in WACCM-D is smaller. This negative difference is more clearly seen in Figures 8 and 9, where we see that mesospheric H_2O anomalies are very consistent between the simulations, except within 10-15 days following the onset of SPE, where the WACCM-D negative anomalies are larger.

3.3 Effect from individual events

The SPE effects are dependent on the background atmosphere and season of the year. Here we discuss this by looking at effects of individual events at selected altitudes. This is also an additional check on the robustness of our analysis.

Figure 10 shows the individual timeseries of differences of epochs from the climatology around 0.05 hPa pressure level (calculated as the mean of three pressure levels centered at 0.04 hPa). SPEs used in this figure are screened for closely separated events, i.e. events which are followed by a larger event within seven days are not shown. Individual events are sorted from top to bottom by the maximum observed proton flux, with strongest events on top of the figure. Dashed horizontal lines show the cut-offs for 1000 pfu (top line) and 100 pfu (bottom line) SPEs.

As expected, the largest SPEs cause a stronger response in O_3, HO_x and NO_x. The response to events is more pronounced in the NH due to the seasonal distribution of SPEs, i.e. there are more events in NH winter. This is especially apparent for NO_x, as its lifetime is heavily influenced by the amount of sunlight available. On visual inspection, the response is dominated by the largest SPEs, with anomalies following the onset of SPEs being visually indistinguishable for the weakest events. Below the 100 pfu threshold, any anomalies following the event onset are dominated by larger events occurring within the analysis period, rather than by the analysed event itself. Thus, the decision to only analyse larger events seems reasonable because the events smaller than 100 pfu would only add a substantial amount of noise to the analysis.

4 Conclusions

We present an analysis of the chemical impacts of SPE on the middle atmosphere using simulations from WACCM-D, a variant of the Whole Atmosphere Community Climate Model including a set of D-region ion chemistry reactions. The aim of our analysis is to study the impact and improvement from a detailed ion chemistry scheme, which is done by comparing

WACCM-D results to those from the standard WACCM scheme which used a simple parameterization of HO_x and NO_x production. Instead of analysing individual SPE events, we present a statistical analysis of the 66 largest SPEs over the years 1989–2012 to allow for more general conclusions in a range of different background atmospheric conditions and with the observed seasonal distribution of SPEs. This statistical approach allowed for the incorporation of smaller events which would have been difficult to analyze separately. Analysis was performed by means of superposed epoch method with bootstrapping to identify statistically robust responses.

Statistically robust SPE signals were present in WACCM-D for all analyzed species (O_3, HO_x, Cl_x, HNO_3, NO_x), except water vapour. These signals are qualitatively in line with previously published modelling results and satellite observations considering individual events. In addition, our analysis shows longer term, solar cycle type signals for several species due to SPEs predominantly occurring during solar maximum years. In general, the responses are consistent between the two hemispheres.

Compared to the standard WACCM, WACCM-D provides solution to some known shortcomings in chemistry-climate models, particularly in the case of HNO_3 and Cl_x response to SPEs. Ozone loss following the SPEs was enhanced at 0.5 hPa in WACCM-D. As there is no corresponding increase of HO_x or NO_x at this altitude, this loss is connected to increased conversion of HCl to reactive Cl_x species by the ion reactions (Winkler et al., 2009), now accounted for in WACCM-D. Conversely, less ozone loss took place around 0.01 hPa in the SH, due to less production of HO_x, in agreement with Andersson et al. (2016). NO_x production in the mesosphere is enhanced by the inclusion of ion chemistry and subsequent downward transport extending the effect to lower altitudes for up to 20 days following the SPE onset. Ion chemistry was found to be crucial for characterization of HNO_3 production following the SPEs which confirms the previous results from 1-D chemistry models (Verronen et al., 2008; Verronen et al., 2011). Some effect was also found in H_2O in an altitude region near the mesopause. This, however, has a large 11-year solar cycle signal, partially masking the SPE impact.

In summary, incomplete representation of EPP-driven chemistry in simulations, for example regarding the HNO_3, has been recognized as one of the outstanding questions in understanding the solar influence in middle atmosphere and below (Jackman et al., 2008; Funke et al., 2011). Our results clearly show the importance of D-region ion chemistry in capturing the effects of energetic particle precipitation in the mesosphere-lower thermosphere simulations. Improved global modeling with ion chemistry such as in WACCM-D, provides an important tool for interpretation of wider range of satellite-based observations of neutral species, and allows for global studies of ionospheric D region.

Code and data availability. All model data used are available from corresponding author by request (niilo.kalakoski@fmi.fi). CESM source code is distributed freely through a public subversion code repository (http://www.cesm.ucar.edu/models/cesm1.0/)

Competing interests. Authors declare that no competing interests are present.

Acknowledgements. This material is based upon work supported in part by the National Center for Atmospheric Research, which is a major facility sponsored by the National Science Foundation under Cooperative Agreement No. 1852977. DRM is also supported by NSF Award #1650918 "Collaborative Research: CEDAR - Quantifying the Impact of Radiation Belt Electron Precipitation on Atmospheric Reactive Nitrogen Oxides (NOx) and Ozone (O3). A.K. is funded by the Tenure Track Project in Radio Science at Sodankylä Geophysical Observatory. Work was carried out as a part of International Space Science Institute (ISSI) project "Space Weather Induced Direct Ionisation Effects On The Ozone Layer".

References

Andersson, M. E., Verronen, P. T., Marsh, D. R., Päivärinta, S.-M., and Plane, J. M. C.: WACCM-D – Improved modeling of nitric acid and active chlorine during energetic particle precipitation, J. Geophys. Res. (Atmos.), 121, 10,328–10,341, https://doi.org/10.1002/2015JD024173, 2016.

5 Calisto, M., Usoskin, I., and Rozanov, E.: Influence of a Carrington-like event on the atmospheric chemistry, temperature and dynamics: revised, Environ. Res. Lett., 8, 045010, https://doi.org/10.1088/1748-9326/8/4/045010, 2013.

Damiani, A., Funke, B., Marsh, D. R., López-Puertas, M., Santee, M. L., Froidevaux, L., Wang, S., Jackman, C. H., von Clarmann, T., Gardini, A., Cordero, R. R., and Storini, M.: Impact of January 2005 solar proton events on chlorine species, Atmos. Chem. Phys., 12, 4159–4179, https://doi.org/10.5194/acp-12-4159-2012, 2012.

10 Denton, M. H., Kivi, R., Ulich, T., Clilverd, M. A., Rodger, C. J., and von der Gathen, P.: Northern hemisphere stratospheric ozone depletion caused by solar proton events: the role of the polar vortex, Geophysical Research Letters, 45, 2115–2124, 2018.

Funke, B., Baumgaertner, A., Calisto, M., Egorova, T., Jackman, C. H., Kieser, J., Krivolutsky, A., López-Puertas, M., Marsh, D. R., Reddmann, T., Rozanov, E., Salmi, S.-M., Sinnhuber, M., Stiller, G. P., Verronen, P. T., Versick, S., von Clarmann, T., Vyushkova, T. Y., Wieters, N., and Wissing, J. M.: Composition changes after the "Halloween" solar proton event: the High-Energy Particle Precipitation in the Atmosphere (HEPPA) model versus MIPAS data intercomparison study, Atmos. Chem. Phys., 11, 9089–9139, https://doi.org/10.5194/acp-11-9089-2011, 2011.

Heino, E., Verronen, P. T., Kero, A., Kalakoski, N., and Partamies, N.: Cosmic noise absorption during solar proton events in WACCM-D and riometer observations, J. Geophys. Res. (Space Phys.), 124, 1361–1376, https://doi.org/10.1029/2018JA026192, 2019.

Jackman, C. H., McPeters, R. D., Labow, G. J., Fleming, E. L., Praderas, C. J., and Russel, J. M.: Northern hemisphere atmospheric effects due to the July 2000 solar proton events, Geophys. Res. Lett., 28, 2883–2886, 2001.

Jackman, C. H., DeLand, M. T., Labow, G. J., Fleming, E. L., Weisenstein, D. K., Ko, M. K. W., Sinnhuber, M., and Russell, J. M.: Neutral atmospheric influences of the solar proton events in October-November 2003, J. Geophys. Res., 110, A09S27, https://doi.org/10.1029/2004JA010888, 2005.

Jackman, C. H., Roble, R. G., and Fleming, E. L.: Mesospheric dynamical changes induced by the solar proton events in October-November 2003, Geophys. Res. Lett., 34, L04 812, https://doi.org/10.1029/2006GL028328, 2007.

Jackman, C. H., Marsh, D. R., Vitt, F. M., Garcia, R. R., Fleming, E. L., Labow, G. J., Randall, C. E., López-Puertas, M., Funke, B., von Clarmann, T., and Stiller, G. P.: Short- and medium-term atmospheric constituent effects of very large solar proton events, Atmos. Chem. Phys., 8, 765–785, https://doi.org/10.5194/acp-8-765-2008, 2008.

Jackman, C. H., Marsh, D. R., Vitt, F. M., Roble, R. G., Randall, C. E., Bernath, P. F., Funke, B., López-Puertas, M., Versick, S., Stiller, G. P., Tylka, A. J., and Fleming, E. L.: Northern Hemisphere atmospheric influence of the solar proton events and ground level enhancement in January 2005, Atmos. Chem. Phys., 11, 6153–6166, https://doi.org/10.5194/acp-11-6153-2011, 2011.

Jackman, C. H., Randall, C. E., Harvey, V. L., Wang, S., Fleming, E. L., López-Puertas, M., Funke, B., and Bernath, P. F.: Middle atmospheric changes caused by the January and March 2012 solar proton events, Atmos. Chem. Phys., 14, 1025–1038, https://doi.org/10.5194/acp-14-1025-2014, 2014.

35 Lamarque, J.-F., Emmons, L., Hess, P., Kinnison, D. E., Tilmes, S., Vitt, F., Heald, C., Holland, E. A., Lauritzen, P., Neu, J., et al.: CAM-chem: Description and evaluation of interactive atmospheric chemistry in the Community Earth System Model, Geoscientific Model Development, 5, 369, 2012.

López-Puertas, M., Funke, B., Gil-López, S., von Clarmann, T., Stiller, G. P., Höpfner, M., Kellmann, S., Fischer, H., and Jackman, C. H.: Observation of NO_x enhancement and ozone depletion in the Northern and Southern Hemispheres after the October-November 2003 solar proton events, J. Geophys. Res., 110, A09S43, https://doi.org/10.1029/2005JA011050, 2005.

Marsh, D. R., Garcia, R. R., Kinnison, D. E., Boville, B. A., Sassi, F., Solomon, S. C., and Matthes, K.: Modeling the whole atmosphere response to solar cycle changes in radiative and geomagnetic forcing, J. Geophys. Res. (Atmos.), 112, D23 306, https://doi.org/10.1029/2006JD008306, 2007.

Marsh, D. R., Mills, M., Kinnison, D., Lamarque, J.-F., Calvo, N., and Polvani, L.: Climate change from 1850 to 2005 simulated in CESM1(WACCM), J. Climate, 26, 7372–7391, https://doi.org/10.1175/JCLI-D-12-00558.1, 2013.

Nieder, H., Winkler, H., D.R., M., and Sinnhuber, M.: NO_x production due to energetic particle precipitation in the MLT region: Results from ion chemistry model studies, J. Geophys. Res. (Space Phys.), 119, 2137–2148, https://doi.org/http://dx.doi.org/10.1002/2013JA019044, 2014.

Orsolini, Y. J., Smith-Johnsen, C., Marsh, D. R., Stordal, F., Rodger, C. J., Verronen, P. T., and Clilverd, M. A.: Mesospheric nitric acid enhancements during energetic electron precipitation events simulated by WACCM-D, J. Geophys. Res. (Atmos.), 123, 6984–6998, https://doi.org/10.1029/2017JD028211, https://doi.org/10.1029/2017JD028211, 2018.

Päivärinta, S.-M., Verronen, P. T., Funke, B., Gardini, A., Seppälä, A., and Andersson, M. E.: Transport versus energetic particle precipitation: Northern polar stratospheric NO_x and ozone in January-March 2012, J. Geophys. Res. (Atmos.), 121, 6085–6100, https://doi.org/10.1002/2015JD024217, 2016.

Pettit, J., Randall, C. E., Marsh, D. R., Bardeen, C. G., Qian, L., Jackman, C. H., Woods, T. N., Coster, A., and Harvey, V. L.: Effects of the September 2005 solar flares and solar proton events on the middle atmosphere in WACCM, J. Geophys. Res. (Space Phys.), 123, 5747–5763, https://doi.org/10.1029/2018JA025294, 2018.

Porter, H. S., Jackman, C. H., and Green, A. E. S.: Efficiencies for production of atomic nitrogen and oxygen by relativistic proton impact in air, J. Chem. Phys., 65, 154–167, 1976.

Rienecker, M. M., Suarez, M. J., Gelaro, R., Todling, R., Bacmeister, J., Liu, E., Bosilovich, M. G., Schubert, S. D., Takacs, L., Kim, G.-K., Bloom, S., Chen, J., Collins, D., Conaty, A., da Silva, A., Gu, W., Joiner, J., Koster, R. D., Lucchesi, R., Molod, A., Owens, T., Pawson, S., Pegion, P., Redder, C. R., Reichle, R., Robertson, F. R., Ruddick, A. G., Sienkiewicz, M., and Woollen, J.: MERRA: NASA's Modern-Era Retrospective Analysis for Research and Applications, Journal of Climate, 24, 3624–3648, https://doi.org/10.1175/JCLI-D-11-00015.1, 2011.

Rozanov, E., Calisto, M., Egorova, T., Peter, T., and Schmutz, W.: The influence of precipitating energetic particles on atmospheric chemistry and climate, Surveys in Geophys., 33, 483–501, https://doi.org/10.1007/s10712-012-9192-0, 2012.

Schmidt, H., Brasseur, G. P., Charron, M., Manzini, E., Giorgetta, M. A., Diehl, T., Fomichev, V. I., Kinnison, D., Marsh, D., and Walters, S.: The HAMMONIA chemistry climate model: Sensitivity of the mesopause region to the 11-year solar cycle and CO2 doubling, J. Climate, 19, 3903–3931, 2006.

Semeniuk, K., Fomichev, V. I., McConnell, J. C., Fu, C., Melo, S. M. L., and Usoskin, I. G.: Middle atmosphere response to the solar cycle in irradiance and ionizing particle precipitation, Atmos. Chem. Phys., 11, 5045–5077, https://doi.org/10.5194/acp-11-5045-2011, 2011.

Seppälä, A., Verronen, P. T., Kyrölä, E., Hassinen, S., Backman, L., Hauchecorne, A., Bertaux, J. L., and Fussen, D.: Solar proton events of October-November 2003: Ozone depletion in the Northern Hemisphere polar winter as seen by GOMOS/Envisat, Geophys. Res. Lett., 31, L19 107, https://doi.org/10.1029/2004GL021042, 2004.

Seppälä, A., Randall, C. E., Clilverd, M. A., Rozanov, E., and Rodger, C. J.: Geomagnetic activity and polar surface air temperature variability, J. Geophys. Res., 114, A10 312, https://doi.org/10.1029/2008JA014029, 2009.

Solomon, S., Rusch, D. W., Gérard, J.-C., Reid, G. C., and Crutzen, P. J.: The effect of particle precipitation events on the neutral and ion chemistry of the middle atmosphere: II. Odd hydrogen, Planet. Space Sci., 8, 885–893, 1981.

5 Stone, K. A., Solomon, S., and Kinnison, D. E.: On the identification of ozone recovery, Geophys. Res. Lett., 45, 5158–5165, https://doi.org/10.1029/2018GL077955, 2018.

Turunen, E., Verronen, P. T., Seppälä, A., Rodger, C. J., Clilverd, M. A., Tamminen, J., Enell, C.-F., and Ulich, T.: Impact of different precipitation energies on NO_x generation during geomagnetic storms, J. Atmos. Sol.-Terr. Phys., 71, 1176–1189, https://doi.org/10.1016/j.jastp.2008.07.005, 2009.

10 Verronen, P. T. and Lehmann, R.: Analysis and parameterisation of ionic reactions affecting middle atmospheric HO_x and NO_y during solar proton events, Ann. Geophys., 31, 909–956, https://doi.org/10.5194/angeo-31-909-2013, 2013.

Verronen, P. T., Seppälä, A., Kyrölä, E., Tamminen, J., Pickett, H. M., and Turunen, E.: Production of odd hydrogen in the mesosphere during the January 2005 solar proton event, Geophys. Res. Lett., 33, L24 811, https://doi.org/10.1029/2006GL028115, 2006.

Verronen, P. T., Funke, B., López-Puertas, M., Stiller, G. P., von Clarmann, T., Glatthor, N., Enell, C.-F., Turunen, E., and Tamminen, J.:
15 About the increase of HNO_3 in the stratopause region during the Halloween 2003 solar proton event, Geophys. Res. Lett., 35, L20 809, https://doi.org/10.1029/2008GL035312, 2008.

Verronen, P. T., Santee, M. L., Manney, G. L., Lehmann, R., Salmi, S.-M., and Seppälä, A.: Nitric acid enhancements in the mesosphere during the January 2005 and December 2006 solar proton events, J. Geophys. Res., 116, D17 301, https://doi.org/10.1029/2011JD016075, 2011.

20 Verronen, P. T., Andersson, M. E., Marsh, D. R., Kovács, T., and Plane, J. M. C.: WACCM-D – Whole Atmosphere Community Climate Model with D-region ion chemistry, J. Adv. Model. Earth Syst., 8, 954–975, https://doi.org/10.1002/2015MS000592, 2016.

von Savigny, C., Sinnhuber, M., Bovensmann, H., Burrows, J., Kallenrode, M.-B., and Schwartz, M.: On the disappearance of noctilucent clouds during the January 2005 solar proton events, Geophysical Research Letters, 34, 2007.

Winkler, H., Kazeminejad, S., Sinnhuber, M., Kallenrode, M.-B., and Notholt, J.: Conversion of mesospheric HCl into active chlorine during
25 the solar proton event in July 2000 in the northern polar region, J. Geophys. Res., 114, D00I03, https://doi.org/10.1029/2008JD011587, 2009.

Winkler, H., Kazeminejad, S., Sinnhuber, M., Kallenrode, M.-B., and Notholt, J.: Correction to "Conversion of mesospheric HCl into active chlorine during the solar proton event in July 2000 in the northern polar region", J. Geophys. Res., 116, D17303, https://doi.org/10.1029/2011JD016274, 2011.

30 Winkler, H., von Savigny, C., Burrows, J. P., Wissing, J. M., Schwartz, M. J., Lambert, A., and García-Comas, M.: Impacts of the January 2005 solar particle event on noctilucent clouds and water at the polar summer mesopause, Atmos. Chem. Phys., 12, 5633–5646, https://doi.org/10.5194/acp-12-5633-2012, 2012.

WMO: Scientific Assessment of Ozone Depletion: 2018, Global Ozone Research and Monitoring Project – Report No. 58, World Meteorological Organization, Geneva, Switzerland, 2018.
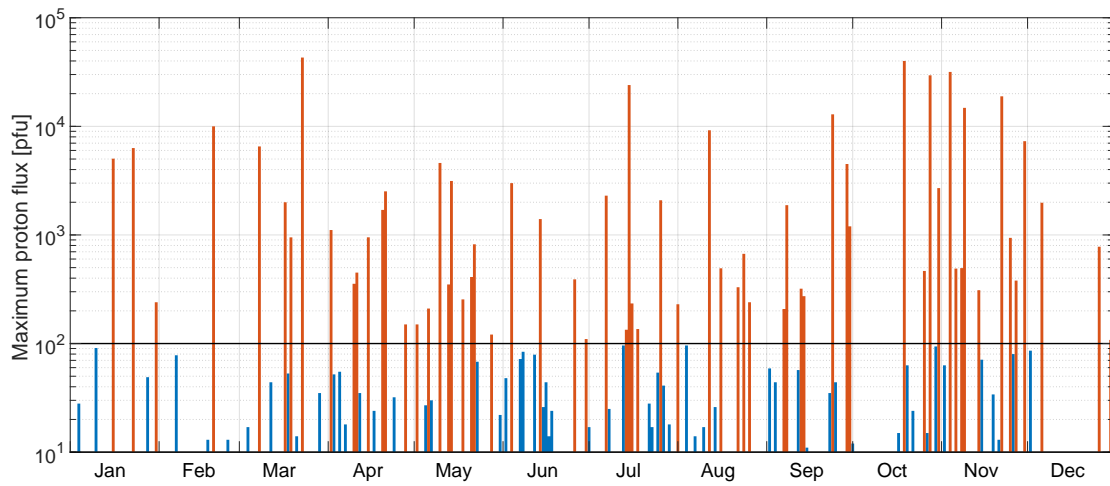
Figure 1. Maximum proton flux of solar proton events used in the analysis as a function of day-of-year of the SPE onset. Events with maximum flux over threshold value (100 pfu) are shown as red bars and smaller events as blue bars.
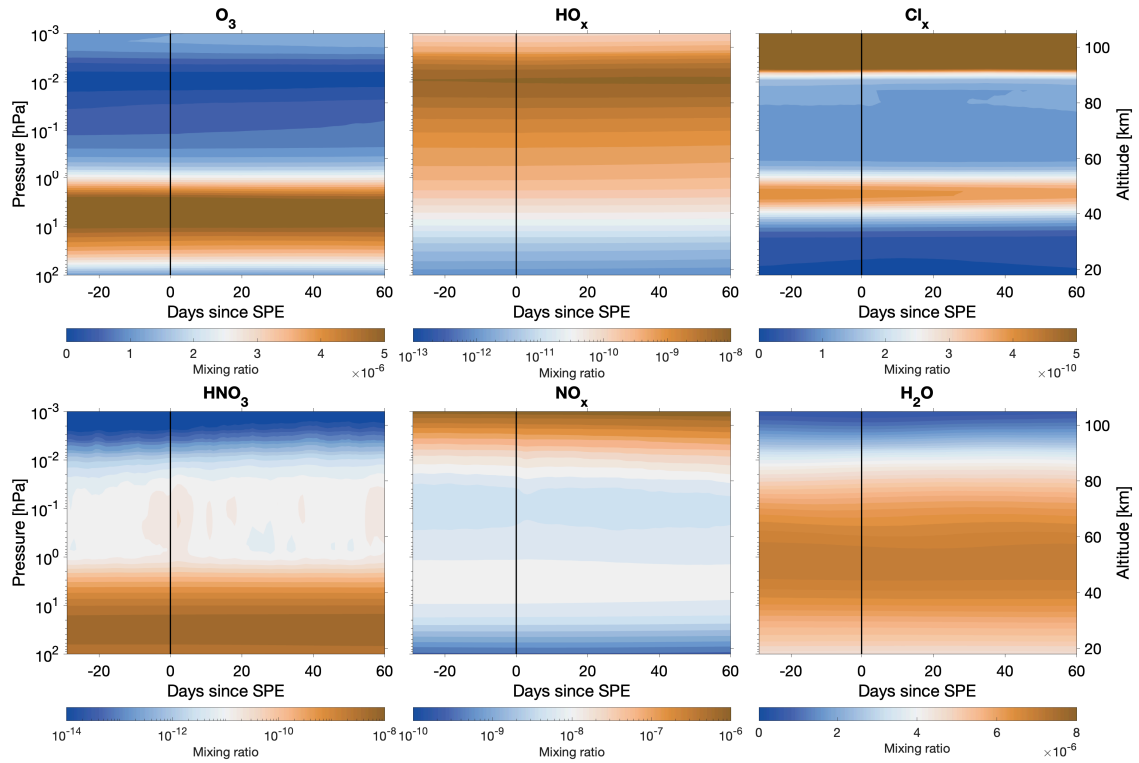
Figure 2. Area-weighted northern polar cap (latitude > 60°N) average of composite mean of $\overline{WD}$ for O_3, HO_x, Cl_x, HNO_3, NO_x and H_2O. X-axis shows the number of days before and after the event (day 0, solid black line) and y-axis pressure levels in model (hPa, left) and approximate altitude (km, right).
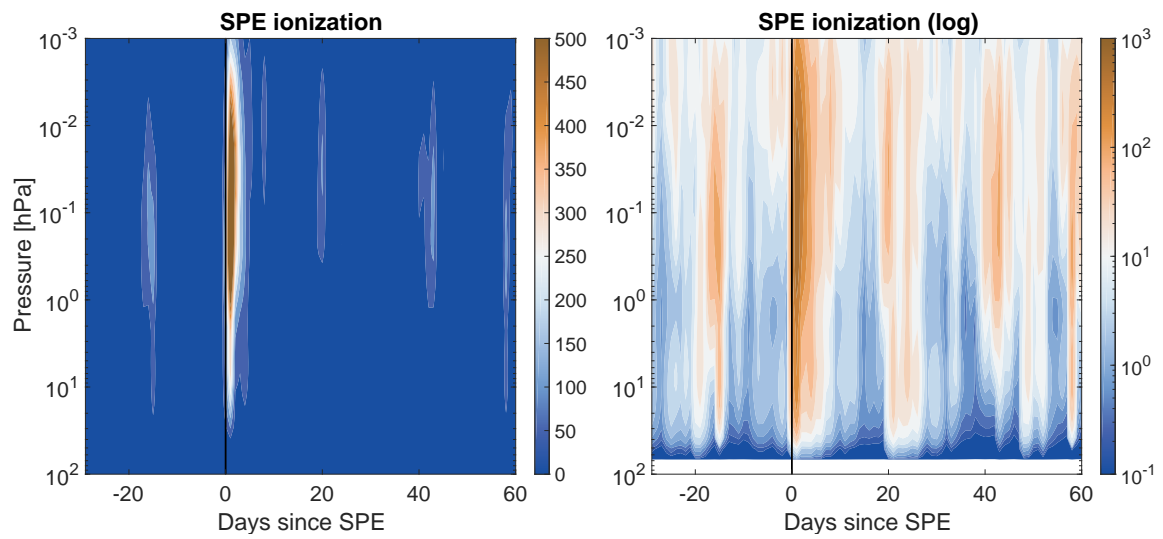
Figure 3. Composite mean of epoch time series of SPE ionization rates in linear (left) and logarithmic (right) color scale. X-axis shows the number of days before and after the event (day 0, solid black line) and y-axis pressure levels in model.
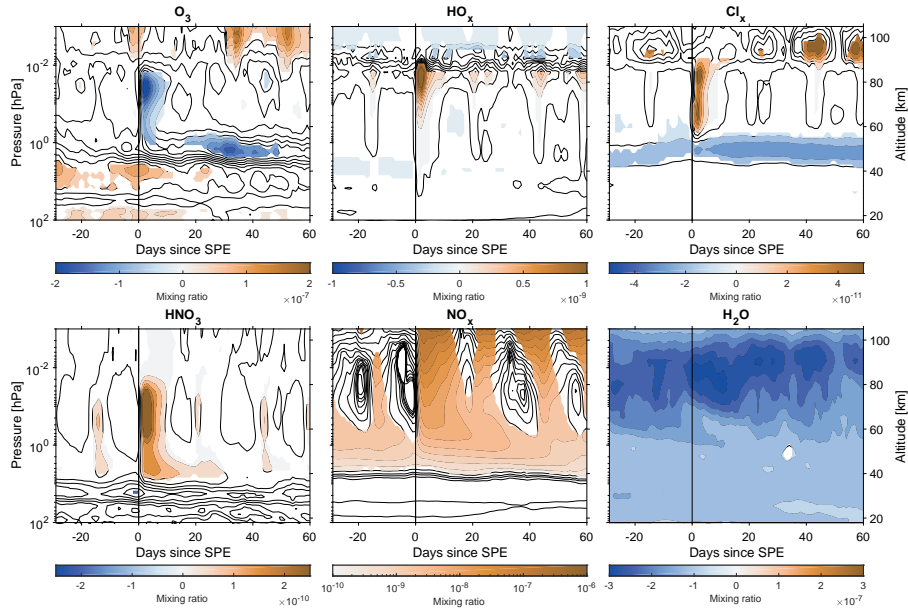
Figure 4. Area-weighted northern polar cap averages (latitude > 60°N) of composite means of $\widehat{WD}$ for O_3, HO_x, Cl_x, HNO_3, NO_x and H_2O. X-axis shows the number of days before and after the event (day 0, solid black line) and y-axis pressure levels in model (hPa, left) and approximate altitude (km, right). Note that the color scale for NO_x panel is logarithmic, and all contours shown in that panel indicate positive difference.
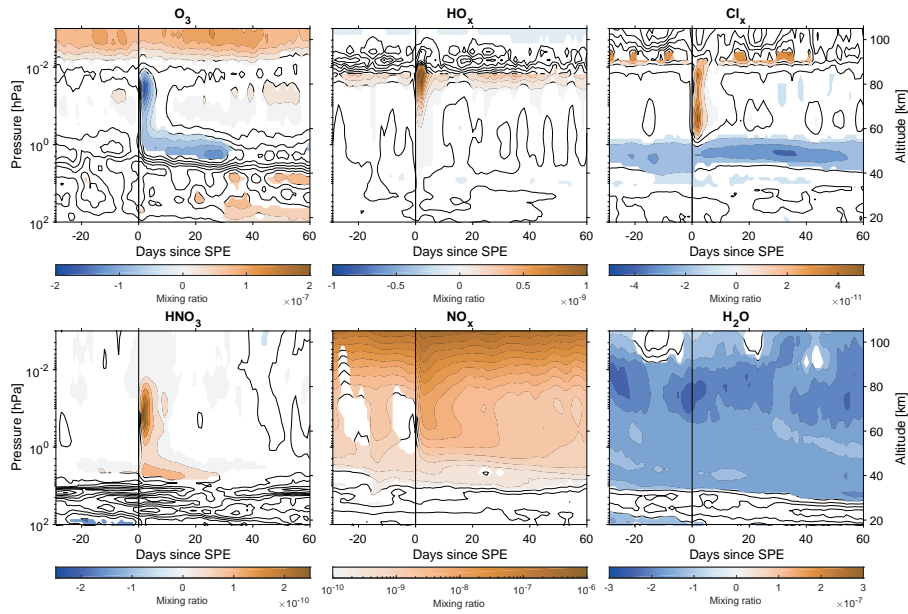
Figure 5. Area-weighted southern polar cap averages (latitude > 60°S) of composite means of $\widehat{WD}$ for O_3, HO_x, Cl_x, HNO_3, NO_x and H_2O. X-axis shows the number of days before and after the event (day 0, solid black line) and y-axis pressure levels in model (hPa, left) and approximate altitude (km, right). Note that the color scale for NO_x panel is logarithmic, and all contours shown in that panel indicate positive difference.
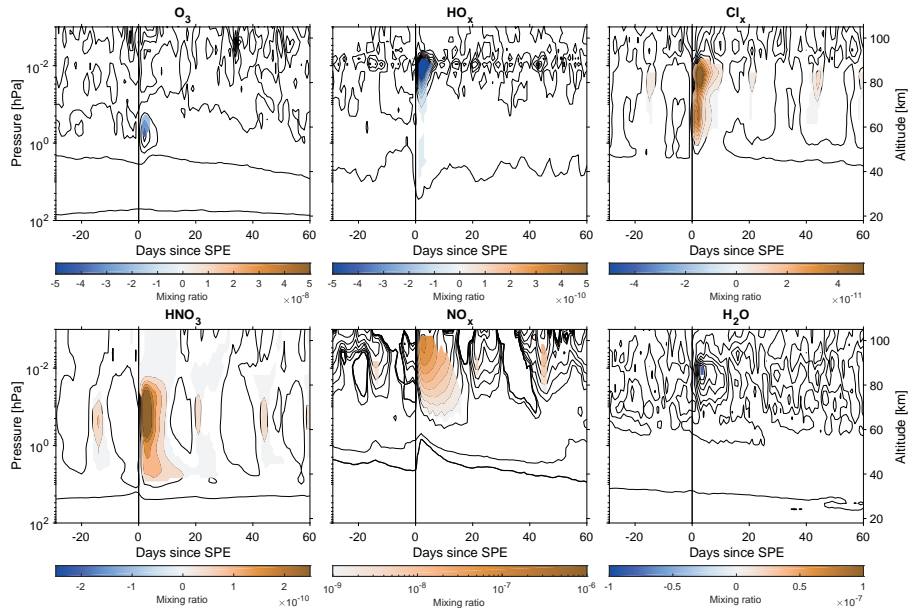
Figure 6. Area-weighted northern polar cap averages (latitude $> 60°N$) of composite means of $\widehat{WD}$ - $\widehat{REF}$ (see figure 4). X-axis shows the number of days before and after the event (day 0, solid black line) and y-axis pressure levels in model (hPa, left) and approximate altitude (km, right). Note that the color scale for NO_x panel is logarithmic, and all contours shown in that panel indicate positive difference.
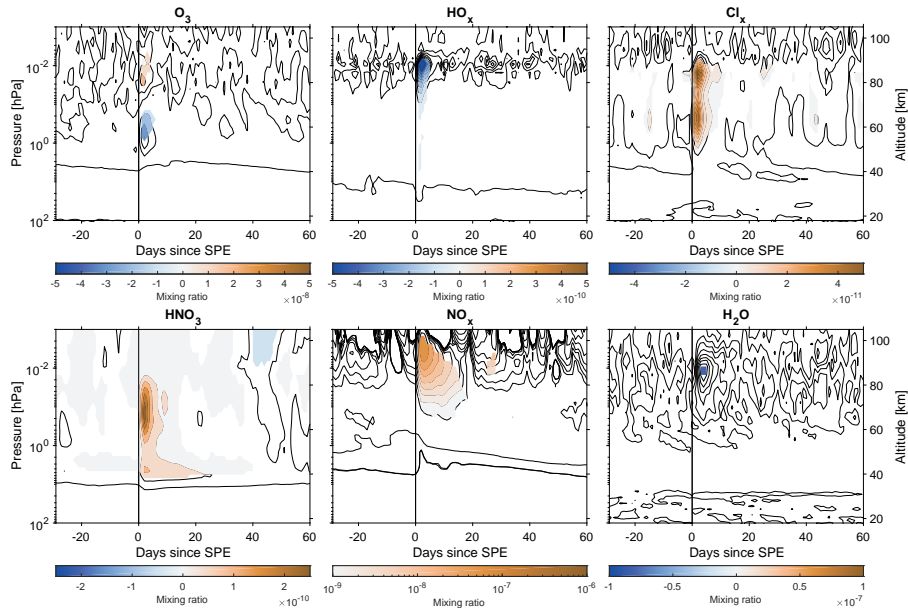
Figure 7. Area-weighted southern polar cap averages (latitude $> 60°\,S$) of composite means of $\widehat{WD}$ - $\widehat{REF}$ (see figure 5). X-axis shows the number of days before and after the event (day 0, solid black line) and y-axis pressure levels in model (hPa, left) and approximate altitude (km, right). Note that the color scale for NO_x panel is logarithmic, and all contours shown in that panel indicate positive difference.
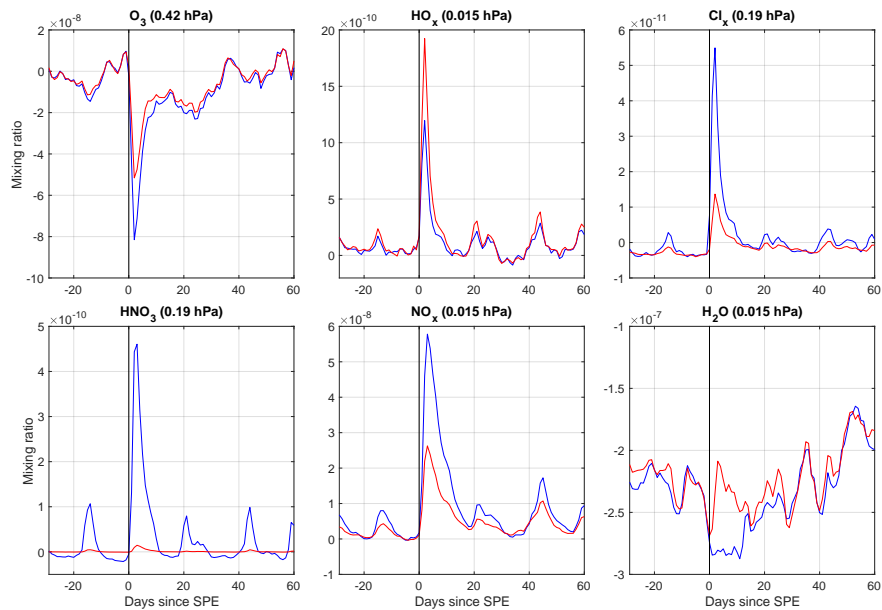
Figure 8. Composite mean $\widehat{WD}$ (blue) and $\widehat{REF}$ (red) for northern polar cap (area-weighted, latitude > 60°N) at selected pressure bands (three pressure levels, pressure of the center of the band shown in panel title). X-axis shows the number of days before and after the event (day 0, solid black line).
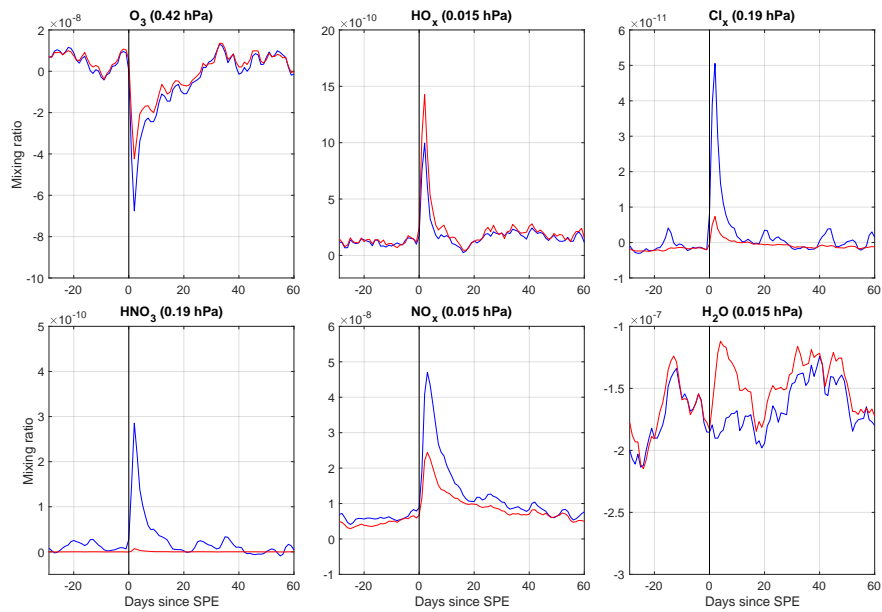
Figure 9. Composite mean $\widehat{\text{WD}}$ (blue) and $\widehat{\text{REF}}$ (red) for southern polar cap (area-weighted, latitude $> 60°$S) at selected pressure bands (three pressure levels, pressure of the center of the band shown in panel title). X-axis shows the number of days before and after the event (day 0, solid black line).
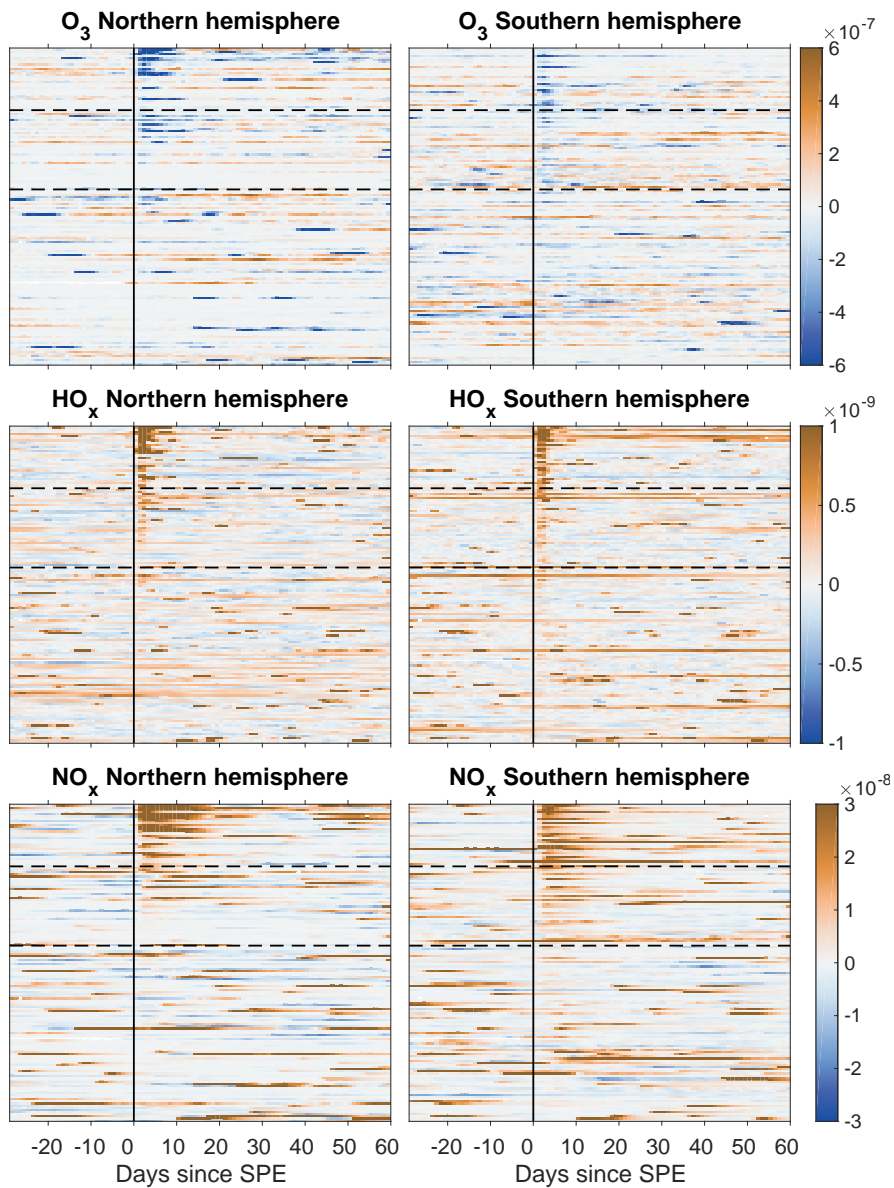
Figure 10. $\widehat{WD}$ of individual SPEs at 0.05 hPa pressure level, sorted by the increasing SPE magnitude for northern (left) and southern (right) polarcaps. Dashed lines represent the 100 (bottom) and 1000 (top) pfu limits.

Table A1. List of solar proton events used in analysis, with their start dates, dates of maximum intensity and the maximum proton fluxes (particle flux unit, $\mathrm{cm}^{-2}\mathrm{s}^{-1}\mathrm{sr}^{-1}$).

Start date	Maximum date	Proton Flux [pfu]	Start date	Maximum date	Proton Flux [pfu]
08-Mar-1989	13-Mar-1989	3500	12-Sep-2000	13-Sep-2000	320
17-Mar-1989	18-Mar-1989	2000	08-Nov-2000	09-Nov-2000	14800
11-Apr-1989	12-Apr-1989	450	24-Nov-2000	26-Nov-2000	940
06-May-1989	06-May-1989	110	02-Apr-2001	03-Apr-2001	1110
12-Aug-1989	13-Aug-1989	9200	10-Apr-2001	11-Apr-2001	355
29-Sep-1989	30-Sep-1989	4500	15-Apr-2001	15-Apr-2001	951
19-Oct-1989	20-Oct-1989	40000	16-Aug-2001	16-Aug-2001	493
27-Nov-1989	28-Nov-1989	380	24-Sep-2001	25-Sep-2001	12900
30-Nov-1989	01-Dec-1989	7300	04-Nov-2001	06-Nov-2001	31700
19-Mar-1990	19-Mar-1990	950	22-Nov-2001	24-Nov-2001	18900
28-Apr-1990	28-Apr-1990	150	26-Dec-2001	26-Dec-2001	779
21-May-1990	22-May-1990	410	21-Apr-2002	21-Apr-2002	2520
01-Aug-1990	01-Aug-1990	230	22-May-2002	23-May-2002	820
31-Jan-1991	31-Jan-1991	240	16-Jul-2002	17-Jul-2002	234
23-Mar-1991	24-Mar-1991	43000	24-Aug-2002	24-Aug-2002	317
13-May-1991	13-May-1991	350	07-Sep-2002	07-Sep-2002	208
04-Jun-1991	11-Jun-1991	3000	09-Nov-2002	10-Nov-2002	404
14-Jun-1991	15-Jun-1991	1400	28-May-2003	29-May-2003	121
30-Jun-1991	02-Jul-1991	110	26-Oct-2003	26-Oct-2003	466
07-Jul-1991	08-Jul-1991	2300	28-Oct-2003	29-Oct-2003	29500
26-Aug-1991	27-Aug-1991	240	25-Jul-2004	26-Jul-2004	2086
09-May-1992	09-May-1992	4600	13-Sep-2004	14-Sep-2004	273
25-Jun-1992	26-Jun-1992	390	07-Nov-2004	08-Nov-2004	495
30-Oct-1992	31-Oct-1992	2700	16-Jan-2005	17-Jan-2005	5040
20-Feb-1994	21-Feb-1994	10000	14-May-2005	15-May-2005	3140
06-Nov-1997	07-Nov-1997	490	14-Jul-2005	15-Jul-2005	134
20-Apr-1998	21-Apr-1998	1700	22-Aug-2005	23-Aug-2005	330
02-May-1998	02-May-1998	150	08-Sep-2005	11-Sep-2005	1880
06-May-1998	06-May-1998	210	06-Dec-2006	07-Dec-2006	1980
24-Aug-1998	26-Aug-1998	670	23-Jan-2012	24-Jan-2012	6310
30-Sep-1998	01-Oct-1998	1200	07-Mar-2012	08-Mar-2012	6530
14-Nov-1998	14-Nov-1998	310	17-May-2012	17-May-2012	255
14-Jul-2000	15-Jul-2000	24000	17-Jul-2012	18-Jul-2012	136